(±6.1%) of all cases, one cell (Fig. 4, H and H_1) accumulated organelles fluorescing in the second color (Fig. 4, I and I_1). With respect to the low percentage of 11.3 (±2.8%) of all cells in culture displaying transfer, this value suggests a strong correlation between organelle transfer and the existence of a TNT connection. The transfer of organelles first became visible 2 hours after coculturing and, at later time points, showed as distinct cells harboring mostly organelles fluorescing in both colors (fig. S12). This indicates fusion of red- and green-labeled structures, a result consistent with reports on early endosomal fusion (*10*). The intercellular, TNT-dependent transfer of labeled organelles was also detected by analyzing mixed cultures of DiI- and DiO-labeled NRK cells (fig. S13). For a pair of TNT-connected cells, only one cell displayed both colors, which suggested transfer in one direction only. A quantitative analysis by fluorescence-activated cell sorting (FACS) revealed that the increase in number of cells with mixed fluorescence correlated with the increase in number of TNTs between cells after plating (fig. S4A). Performing transfer experiments close to 0°C, conditions that block exo-, endo-, or phagocytotic events (*11, 12*), we still detected organelle transfer between TNT-connected cells (fig. S14). Thus, the observed transfer did not depend on conventional exo-, endo-, or phagocytotic events. Organelle exchange could be blocked in the presence of latrunculin-B (fig. S14E), which strongly supported the presence of an actin-based transfer mechanism.

The observation that functional TNTs were also found in cell cultures of lineages other than neuroendocrine cells (figs. S1 and S13) raises the possibility that TNTs represent a general cellular phenomenon occurring in long-range cell-to-cell communication. The transfer of endosome-related structures through TNTs is consistent with the finding that similar structures, termed argosomes, facilitate the intercellular spread of wingless morphogens (*13*). Argosomes are thought to be exchanged between cells via sequential exo- and endocytotic events (*14*). The transfer of melanosomes between melanocytes and keratinocytes represents another riddle of organelle exchange (*15*). It has been proposed that this transfer occurs by means of local membrane fusion or phagocytotic mechanisms (*15*). Our finding that cells can actively exchange small membrane carriers through membrane channels provides evidence for a new principle of cell-to-cell communication based on membrane continuity between TNT-connected cells (Fig. 4, J and K). Provided that TNTs are present in tissue, reconsideration of previous interpretations of intercellular communication may be necessary. In this respect, the concept of membrane continuity between animal cells may also facilitate cell-to-cell transport of, e.g., transcription factors or ribonucleoparticles, as has been documented for the plant kingdom (*16, 17*).

References and Notes

1. Materials and methods are available as supporting material on *Science* Online.
2. F. A. Ramirez-Weber, T. B. Kornberg, *Cell* **97**, 599 (1999).
3. A. Karlsson *et al*., *Nature* **409**, 150 (2001).
4. M. J. Hannah, A. A. Schmidt, W. B. Huttner, *Annu. Rev. Cell Dev. Biol.* **15**, 733 (1999).
5. V. Mermall, P. L. Post, M. S. Mooseker, *Science* **279**, 527 (1998).
6. D. A. Schafer *et al*., *J. Cell Biol.* **143**, 1919 (1998).
7. R. J. Pelham Jr., F. Chang, *Nature Cell Biol.* **3**, 235 (2001).
8. M. G. Honig, R. I. Hume, *Trends Neurosci.* **12**, 333 (1989).
9. D. P. Kuffler, *J. Comp. Neurol.* **302**, 729 (1990).
10. J. P. Gorvel, P. Chavrier, M. Zerial, J. Gruenberg, *Cell* **64**, 915 (1991).
11. I. H. Pastan, M. C. Willingham, *Science* **214**, 504 (1981).
12. M. Desjardins, L. A. Huber, R. G. Parton, G. Griffiths, *J. Cell Biol.* **124**, 677 (1994).
13. V. Greco, M. Hannus, S. Eaton, *Cell* **106**, 633 (2001).
14. K. Denzer, M. J. Kleijmeer, H. F. Heijnen, W. Stoorvogel, H. J. Geuze, *J. Cell Sci.* **113**, 3365 (2000).
15. G. Scott, S. Leopardi, S. Printup, B. C. Madden, *J. Cell Sci.* **115**, 1441 (2002).
16. K. Nakajima, G. Sena, T. Nawy, P. N. Benfey, *Nature* **413**, 307 (2001).
17. W. Lucas, B.-C. Yoo, F. Kragler, *Nature Rev. Mol. Cell Biol.* **2**, 849 (2001).

18. We thank A. Hellwig for generous help in electron microscopy, A. Kehlenbach and B. Schwappach for FACS analysis, J. Hammer for providing Dil2 antibody, A. Matus for providing EGFP-actin, R. Leube for providing synaptophysin-EGFP, and W. Franke and J. Leichtle for valuable comments on the manuscript. I.M. was supported by the Coimbra Group Hospitality Scheme and A.R. by the Landesgraduiertenstipendium Baden-Württemberg; H.-H.G. was a recipient of grants from the Deutsche Forschungsgemeinschaft (SFB 488/B2, GE 550/3-2).

Supporting Online Material

www.sciencemag.org/cgi/content/full/303/5660/1007/DC1
Materials and Methods
Figs. S1 to S14
Movies S1 to S8
References

30 October 2003; accepted 10 December 2003

Direct Activation of Bax by p53 Mediates Mitochondrial Membrane Permeabilization and Apoptosis

Jerry E. Chipuk,[1] Tomomi Kuwana,[1] Lisa Bouchier-Hayes,[1] Nathalie M. Droin,[1] Donald D. Newmeyer,[1] Martin Schuler,[2] Douglas R. Green[1]*

The tumor suppressor p53 exerts its anti-neoplastic activity primarily through the induction of apoptosis. We found that cytosolic localization of endogenous wild-type or trans-activation–deficient p53 was necessary and sufficient for apoptosis. p53 directly activated the proapoptotic Bcl-2 protein Bax in the absence of other proteins to permeabilize mitochondria and engage the apoptotic program. p53 also released both proapoptotic multidomain proteins and BH3-only proteins [Proapoptotic Bcl-2 family proteins that share only the third Bcl-2 homology domain (BH3)] that were sequestered by Bcl-xL. The transcription-independent activation of Bax by p53 occurred with similar kinetics and concentrations to those produced by activated Bid. We propose that when p53 accumulates in the cytosol, it can function analogously to the BH3-only subset of proapoptotic Bcl-2 proteins to activate Bax and trigger apoptosis.

The induction of apoptosis is central to the tumor-suppressive activity of p53 (*1*). Upon activation by DNA damage–induced or oncogene-induced signaling pathways, p53 promotes the expression of a number of genes that are involved in apoptosis, including those encoding death receptors (*2*, *3*) and proapoptotic members of the Bcl-2 family (*4*, *5*). In most cases, p53-induced apoptosis proceeds through mitochondrial release of cytochrome c, which leads to caspase activation (*6*).

Although most of the effects of p53 are ascribed to its function as a transcription factor, reports have suggested that the protein can also induce apoptosis independently of new protein synthesis (*7–10*). However, these studies have relied on ectopic expression of p53 or overexpression of mutants that lack transcriptional activity. Transcription-independent induction of apoptosis by p53 requires Bax and involves cytochrome c release and caspase activation, all of which occur in the absence of a nucleus, suggesting that p53 has the capacity to engage the apoptotic program directly from the cytoplasm (*11*).

We therefore tested if endogenous p53 can engage the apoptotic program directly

[1]Division of Cellular Immunology, La Jolla Institute for Allergy and Immunology, 10355 Science Center Drive, San Diego, CA 92121, USA. [2]Department of Medicine III, Johannes Gutenberg University, D-55101 Mainz, Germany.

*To whom correspondence should be addressed. E-mail: doug@liai.org

from the cytoplasm in the absence of p53-induced transcription. We used E1A/H-rasG12V–transformed wild-type p53 ($p53^{wt}$), $Bax^{-/-}$, and $p53^{-/-}$ mouse embryonic fibroblasts (MEF) and an inhibitor of nuclear import, wheat germ agglutinin (WGA). p53 accumulated in both the nucleus and cytoplasm of $p53^{wt}$ and $Bax^{-/-}$ MEF that were exposed to ultraviolet (UV) light; however, pretreatment of cells with WGA blocked the nuclear import of p53 such that p53 was found exclusively in the cytoplasm (Fig. 1A). WGA effectively inhibited UV-induced p53-dependent induction of several p53-responsive genes, assayed by real-time polymerase chain reaction (PCR) (*mdm2*, *bax*, *p21*$^{WAF1/CIP1}$, and *PUMA*; fig. S1A) and Western blot (Bax and $p21^{WAF1/CIP1}$; fig. S1B). Whereas p53-dependent gene expression was blocked by the inhibition of p53 nuclear accumulation, the induction of apoptosis by UV (UV dose responses in fig. S2) proceeded in $p53^{wt}$ MEF even though p53 was exclusively cytoplasmic (Fig. 1B). In contrast, $Bax^{-/-}$ MEF were resistant to UV-induced apoptosis in the presence of WGA, suggesting that cytosolic p53 cooperates with Bax to induce apoptosis in the absence of p53-dependent gene regulation (Fig. 1B). The expression of a sublethal concentration of Bax rescued apoptosis under these conditions (Fig. 1C). The decrease in apoptosis following UV with WGA may represent the requirement for p53-dependent regulation of PUMA (*12*–*14*) or other apoptosis-promoting proteins in the cells without WGA. UV-induced apoptosis without WGA was observed in $Bax^{-/-}$ MEF (Fig. 1B) suggesting that transcription-dependent death is not Bax dependent in these cells.

We analyzed a transcriptionally inactive form of p53 that exclusively displays nuclear localization and does not support p53-dependent apoptosis (*15*). We reasoned that this mutant, $Trp53^{L25Q,W26S}$ (referred to as $p53^{QS}$), might not induce apoptosis because it failed to be exported to the cytosol. When primary untransformed $p53^{QS}$ knock-in MEF were treated with WGA, $p53^{QS}$ was present in both the cytosol and nucleus (Fig. 1D). The cytosolic accumulation of $p53^{QS}$ was associated with cell death even in the absence of UV exposure (Fig. 1E). We speculate that wild-type p53 does not induce death upon WGA treatment without UV because of its proper regulation by MDM2 and other proteins, whereas $p53^{QS}$ accumulates with WGA alone (and therefore triggers apoptosis). As controls, wild-type MEF (primary and transformed) responded to 5-mJ UV by p53-dependent gene regulation and apoptosis (Fig. 1, B and E, and figs. S1 and S2), whereas $p53^{-/-}$ MEF were resistant to 5-mJ UV and WGA-induced effects (Figs. 1, B and E, and figs. S1 and S2).

These results suggest that it is the failure of p53 to localize in the cytosol, rather than a defect in p53-induced transcription of proapoptotic genes, that accounts for the loss of p53-mediated apoptosis in $p53^{QS}$ cells. Indeed, a stably expressed temperature-sensitive form of $p53^{QS}$, localized to the cytosol, was reported to induce apoptosis upon stabilization (*10*). To test the direct cytoplasmic effects of p53 in the absence of p53-induced gene expression, $p53^{UVIP}$, $p53^{\Delta PP}$ (no proline-rich domain, amino acids 62 to 91), and $p53^{QS}$ were purified (fig. S3, A and B) and microinjected into HeLa cells stably expressing a cytochrome c–green fluorescent protein (GFP) fusion protein localized to mitochondria (*16*). To prevent new protein expression in response to p53 or p53 nuclear import, cycloheximide (CHX) or WGA was added, respectively. Although injection of immunoprecipitates from non–UV-treated cell lysates lacking p53 had no effect on these cells (or on isolated mitochondria, fig. S3D), $p53^{UVIP}$ and $p53^{QS}$ each induced cytochrome c release in the microinjected cells (Fig. 2A, quantitation in fig. S3C). Microinjected $p53^{\Delta PP}$ failed to induce cytochrome c release (Fig. 2A and fig. S3C). The amounts of microinjected proteins were in the range of 4 to 40 fg per cell, consistent with the amount of p53 that was isolated from the cytosols of UV-treated MCF-7 cells (*17*).

During apoptosis, the release of cytochrome c and other proteins from the mitochondrial intermembrane space is controlled by the Bcl-2 family of proteins (*18*). A subset of these proteins, including Bid and Bim, share the third Bcl-2 homology domain (BH3) with other family members, and thus are called "BH3-only" proteins. These proteins activate another set of proteins, including Bax and Bak, which contain three of the BH domains ("BH123" or "multidomain" proteins), to permeabilize the mitochondrial outer membrane leading to the release of cytochrome c and other proteins from the intermembrane space. Apoptosis induced by p53 is dependent on Bax and Bak (*19*), and the lack of Bax in MEF partially circumvents p53-mediated suppression of transformation by oncogenes (*4*, *20*, *21*).

Thus, we examined the effect of p53 on isolated mitochondria with and without Bax. Neither recombinant monomeric Bax nor native $p53^{UVIP}$ induced cytochrome c release on its own; however, incubation of mitochondria with both proteins caused cytochrome c release (Fig. 2B). Highly purified, non–stress induced, baculovirus-expressed p53 ($p53^{Bac}$) also induced cytochrome c release in the presence of Bax (Fig. 2C). These results suggest that neither stress-associated p53 modifications nor other proteins synthesized or

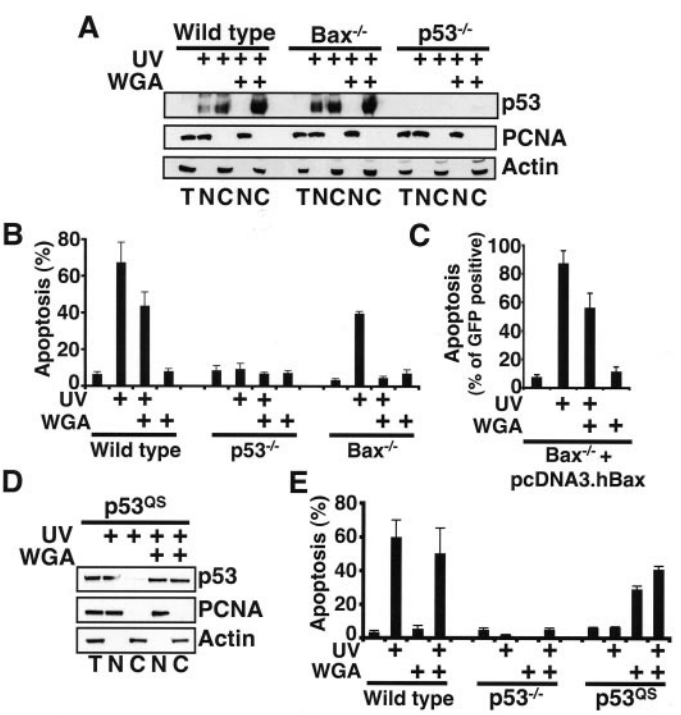

Fig. 1. Cooperation of endogenous cytoplasmic p53 with Bax to induce apoptosis in the absence of p53 nuclear activity. (**A**) UV-induced nuclear accumulation of p53 is blocked by WGA. E1A/H-rasG12V–expressing $p53^{wt}$, $Bax^{-/-}$, and $p53^{-/-}$ MEF were transfected with WGA by means of the Chariot protein delivery system (20 μg WGA per 100-mm^2 plate), treated with 5-mJ UV for 8 hours, and processed into total (T), nuclear (N), and cytoplasmic (C) fractions before immunoprecipitation with an antibody to p53. Starting materials for the immunoprecipitations were subjected to Western blot for proliferating cell nuclear antigen (PCNA, a nuclear marker) and actin (a cytoplasmic marker). (**B**) UV-induced cytosolic p53 failed to induce apoptosis in the absence of Bax. Above MEF were treated as indicated, harvested, and stained with Annexin V–FITC before fluorescence-activated cell sorting analysis (FACS). (**C**) UV-induced cytoplasmic p53-initiated apoptosis was rescued after re-expression of Bax. $Bax^{-/-}$ MEF were transfected with a sublethal dose of Bax, cultured for 24 hours, and treated as indicated before Annexin V–FITC staining and FACS analysis. (**D** and **E**) Inhibition of nuclear import allows for trans-activation–deficient p53 ($p53^{QS}$) to accumulate in the cytosol and induce death. Primary untransformed MEF were treated as described in (A) and (B).

activated upon stress are required for this p53 effect. Although the mouse liver mitochondria have associated Bak (*22*), this appeared to be insufficient to support the p53-induced cytochrome c release. Therefore, this previously unobserved cytoplasmic activity of p53 seems to require Bax.

A fusion protein composed of p53 and the steroid-binding domain of the estrogen receptor, mutated to respond to tamoxifen (p53ER^{tam}), functions in cells to trigger p53-dependent gene expression and apoptosis (*23*). We observed that the transient expression of this fusion protein in transformed wild-type MEF caused apoptosis upon addition of 4-hydroxytamoxifen (4-OHT), which was not inhibited by CHX (fig. S4A). A mutant form of p53 lacking the proline-rich domain (p53$^{\Delta PP}$ER^{tam}) failed to induce apoptosis with and without 4-OHT. p53ER^{tam}, expressed in MEF lacking either Bax alone or Bax and Bak, did not trigger cell death unless Bax was ectopically expressed at subapoptotic levels (fig. S4B). Therefore, the transcription-independent activity of p53 appears to be more dependent on Bax in MEF, as suggested by our previous studies (*11*).

Purified p53ER^{tam} or p53$^{\Delta PP}$ER^{tam} incubated with mitochondria had no effect with or without 4-OHT (Fig. 2D). However, mitochondria released cytochrome c when incubated with recombinant Bax plus active p53ER^{tam} (i.e., with 4-OHT); the p53$^{\Delta PP}$ER^{tam} lacked this effect. Therefore, the function of p53ER^{tam} on Bax appears to require the proline-rich domain of the p53 molecule.

We also tested the effect of p53 on the membrane permeabilizing activity of Bax in a lipid vesicle system that faithfully mimics mitochondrial outer membrane permeabilization (*24*). No effects of recombinant monomeric Bax, recombinant activated Bid (Bid$^{N/C}$), p53^{UVIP}, or p53^{Bac} were observed on the release of labeled dextrans from liposomes when added alone, whereas the addition of Bax and Bid$^{N/C}$ together permeabilized the liposomes (*24*). The addition of native p53^{UVIP} with Bax also caused permeabilization of the liposomes and release of fluorescein isothiocyanate (FITC)–dextran. In the liposome system, 5 nM p53^{UVIP} or p53^{Bac} was effective (Fig. 3A); similar concentrations permeabilized isolated mitochondria (Fig. 2, B and C). In contrast, p53$^{\Delta PP}$ had substantially reduced permeabilization activity in this system (Fig. 3B). p53ER^{tam} also functioned in the liposome system; as little as 130 pM p53ER^{tam} showed effects in the presence of 4-OHT and recombinant Bax (fig. S5). In contrast, the p53$^{\Delta PP}$ER^{tam} mutant had no effect with or without 4-OHT.

We then examined the activation of Bax as indicated by Bax oligomerization (*25*) after treatment with p53 in the liposome system with the cross-linking reagent, 1,6-bismaleimidohexane (BMH). Bax oligomers were induced by all wild-type p53 proteins and p53^{QS}, similar to Bid$^{N/C}$ at equimolar concentrations (Fig. 3C); both p53$^{\Delta PP}$ and p53$^{\Delta PP}$ER^{tam} failed to induce Bax oligomers.

Two proteins, Bid and Bim, activate Bax in this manner, and both are BH3-only members of the Bcl-2 family (*19*, *26*). These are thought to act in a "hit-and-run" manner to induce a conformational change, triggering their oligomerization (*27*). We were unable to detect a physical binding of p53 and Bax (*22*). However, BH3-only proteins, including Bid and Bim, bind to Bcl-2 and Bcl-xL (*26*), and the latter proteins block apoptosis through the sequestration of proapoptotic Bcl-2 members. Some BH3-only proteins (e.g., Bad) do not activate Bax, but instead appear to promote apoptosis by releasing Bid and Bim from Bcl-2 or Bcl-xL (*25*, *28*).

p53 has been reported to bind to Bcl-xL and Bcl-2 (*9*), which might allow for Bak activation by releasing it from these inhibitors. Although p53 could activate Bax in the absence of any other proteins (Fig. 3), we tested if p53 has this additional BH3-like activity to release proapoptotic proteins sequestered by Bcl-xL. For this experiment, we used p53ER^{tam} to determine if this binding might depend on p53 conformation. p53ER^{tam} but not the p53$^{\Delta PP}$ER^{tam} mutant was bound by glutathione *S*-transferase (GST)–Bcl-xL only in the presence of 4-OHT (Fig. 4A). Endogenous Bcl-xL was associated with immunoprecipitated active p53ER^{tam} (Fig. 4B), and this association required the p53 proline-rich domain. Such binding released Bid$^{N/C}$ or Bax that was previously bound to Bcl-xL (Fig. 4C). Native p53 displaced Bid$^{N/C}$ or Bax sequestered by Bcl-xL at an equimolar concentration (Fig. 4D), whereas concentrations of Bid$^{N/C}$ or Bax that were 50 times higher were required to effectively displace native p53 from Bcl-xL (Fig. 4E).

The capacity of p53 to directly activate Bax to permeabilize mitochondria permits an uninterrupted pathway leading from DNA damage, for example, to the mitochondrial release of cytochrome c, caspase activation, and apoptosis. The previously unobserved

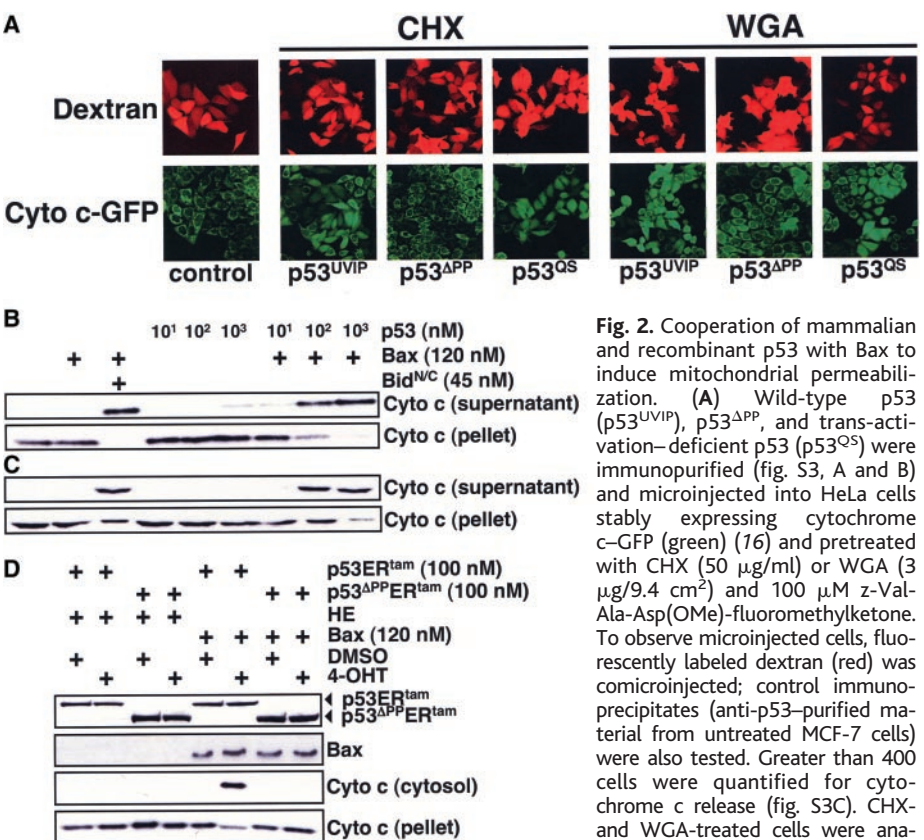

Fig. 2. Cooperation of mammalian and recombinant p53 with Bax to induce mitochondrial permeabilization. (**A**) Wild-type p53 (p53^{UVIP}), p53$^{\Delta PP}$, and trans-activation–deficient p53 (p53^{QS}) were immunopurified (fig. S3, A and B) and microinjected into HeLa cells stably expressing cytochrome c–GFP (green) (*16*) and pretreated with CHX (50 μg/ml) or WGA (3 μg/9.4 cm^2) and 100 μM z-Val-Ala-Asp(OMe)-fluoromethylketone. To observe microinjected cells, fluorescently labeled dextran (red) was comicroinjected; control immunoprecipitates (anti-p53–purified material from untreated MCF-7 cells) were also tested. Greater than 400 cells were quantified for cytochrome c release (fig. S3C). CHX- and WGA-treated cells were analyzed 4 hours postinjection. (**B** and **C**) Effects of p53 on isolated mitochondria. Immunopurified p53^{UVIP} (B) or p53^{Bac} (C) was added to freshly isolated C57Bl/6 liver mitochondria (*30*) with and without recombinant full-length Bax (*31*) and incubated at 37°C for 60 min. Supernatants and mitochondrial pellets were then analyzed for cytochrome c by Western blot. The combination of Bax and Bid$^{N/C}$ is a positive control for mitochondrial permeabilization. (**D**) Immunopurified p53ER^{tam} or p53$^{\Delta PP}$ER^{tam} (fig. S3, A and B) was analyzed with or without 4-OHT for mitochondrial permeabilization as in (B). 10 mM 4-(2-hydroxyethyl) piperazine-1-ethanesulfonic acid pH 7.4, 1 mM ethylenediaminetetraacetic acid (HE) is the buffer for recombinant proteins. DMSO, dimethyl sulfoxide.

function of p53, which is analogous to that of a BH3-only protein, in addition to its function as a transcription factor, demonstrates an emerging complexity that exists within components of the apoptotic machinery. Other examples include cytochrome c, which functions both in electron transfer and caspase activation, and Bcl-2 family members that have roles in the regulation of metabolism that are distinct from their apoptotic function (*29*). This multifunctionality of proteins is a source of complexities that, together with those governing gene regulation and RNA splicing, serve as controls in life-long decisions concerning cellular proliferation, differentiation, and death.

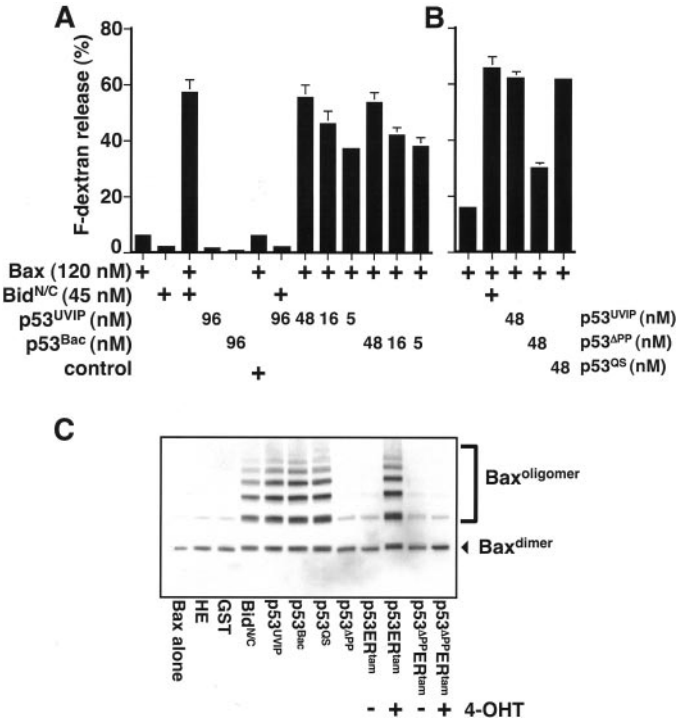

Fig. 3. Cooperation of mammalian and recombinant p53 with Bax to permeabilize synthetic liposomes. (**A** and **B**) Liposomes formed from defined lipid mixtures containing fluorescein (F)–dextran (*24*) were combined with indicated concentrations of p53^{UVIP}, p53^{Bac}, p53$^{\Delta PP}$, or p53^{QS} with and without recombinant full-length Bax (*31*). The combination of Bax and Bid$^{N/C}$ is a positive control for liposome permeabilization. Maximal release is determined by 1% CHAPS solubilization of liposomes. (**C**) Liposomes were combined with full-length Bax (0.25 ng) and either 45 nM p53 (all types indicated) or Bid$^{N/C}$ in the presence of 1 nM BMH before SDS–polyacrylamide gel electrophoresis (PAGE) and Western blot analysis for Bax. Recombinant monomeric Bax (determined by gel filtration) is primarily dimeric after SDS-PAGE analysis (*25*).

References and Notes

1. C. A. Schmitt *et al*., *Cancer Cell* **1**, 289 (2002).
2. L. B. Owen-Schaub *et al*., *Mol. Cell. Biol.* **15**, 3032 (1995).
3. M. Muller *et al*., *J. Exp. Med.* **188**, 2033 (1998).
4. T. Miyashita, J. C. Reed, *Cell* **80**, 293 (1995).
5. E. Oda *et al*., *Science* **288**, 1053 (2000).
6. M. Schuler, E. Bossy-Wetzel, J. C. Goldstein, P. Fitzgerald, D. R. Green, *J. Biol. Chem.* **275**, 7337 (2000).
7. M. Bennett *et al*., *Science* **282**, 290 (1998). Y N
8. C. Caelles, A. Helmberg, M. Karin, *Nature* **370**, 220 (1994).
9. M. Mihara *et al*., *Mol. Cell* **11**, 577 (2003).
10. J. M. Kokontis, A. J. Wagner, M. O'Leary, S. Liao, N. Hay, *Oncogene* **20**, 659 (2001).
11. J. E. Chipuk, U. Maurer, D. R. Green, M. Schuler, *Cancer Cell* **4**, 371 (2003).
12. J. Yu, Z. Wang, K. W. Kinzler, B. Vogelstein, L. Zhang, *Proc. Natl. Acad. Sci. U.S.A.* **100**, 1931 (2003).
13. J. R. Jeffers *et al*., *Cancer Cell* **4**, 321 (2003).
14. A. Villunger *et al*., *Science* **302**, 1036 (2003); published online 18 September 2003 (10.1126/science.1090072).
15. G. S. Jimenez *et al*., *Nat. Genet.* **26**, 37 (2000).
16. J. C. Goldstein, N. J. Waterhouse, P. Juin, G. I. Evan, D. R. Green, *Nat. Cell Biol.* **2**, 156 (2000).
17. Materials and methods are available as supporting material on *Science* Online.
18. R. M. Kluck, E. Bossy-Wetzel, D. R. Green, D. D. Newmeyer, *Science* **275**, 1132 (1997).

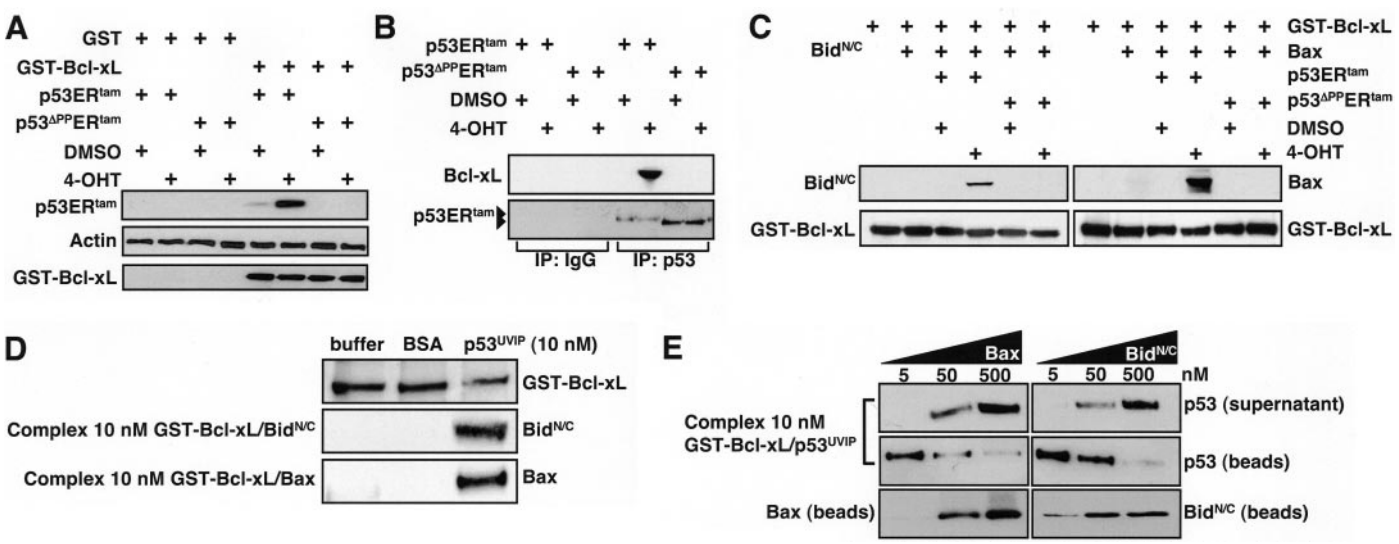

Fig. 4. Liberation of proapoptotic Bcl-2 proteins sequestered by Bcl-xL after interaction with p53. (**A**) Active p53ER^{tam} but not p53$^{\Delta PP}$ER^{tam} directly binds recombinant Bcl-xL. p53ER^{tam} or p53$^{\Delta PP}$ER^{tam} cytosols were combined with GST–Bcl-xL with or without 100 nM 4-OHT. Complexes were detected by SDS-PAGE and Western blot analysis. (**B**) Active p53ER^{tam} but not p53$^{\Delta PP}$ER^{tam} binds to endogenous Bcl-xL. H1299 cells stably expressing p53ER^{tam} or p53$^{\Delta PP}$ER^{tam} were treated with or without 100 nM 4-OHT for 24 hours and the p53ER^{tam} or p53$^{\Delta PP}$ER^{tam} was immunoprecipitated. Complexes were detected by SDS-PAGE and Western blot analysis. (**C**) Release of full-length Bax or Bid$^{N/C}$ complexed with Bcl-xL in the presence of p53ER^{tam} but not p53$^{\Delta PP}$ER^{tam}. Immunopurified p53ER^{tam} or p53$^{\Delta PP}$ER^{tam} was combined with complexes of GST–Bcl-xL/Bax or GST–Bcl-xL/Bid$^{N/C}$ with or without 100 nM 4-OHT. Liberated proteins were detected by SDS-PAGE and Western blot analysis. (**D**) Release of full-length Bax or Bid$^{N/C}$ complexed with Bcl-xL in the presence of a low concentration of native p53^{UVIP}. GST–Bcl-xL (10 nM) was incubated with 100 nM Bid$^{N/C}$ or Bax and washed to remove all unbound protein; 10 nM p53 [or bovine serum albumin (BSA)] was added. Liberated proapoptotic proteins were detected. (**E**) The association between Bcl-xL and p53 is disrupted by Bax or Bid$^{N/C}$ only at high molar excess. GST–Bcl-xL (10 nM) was incubated with 100 nM p53^{UVIP} and washed to remove all unbound protein. Indicated concentrations of Bax or Bid$^{N/C}$ were added. Liberated p53 was detected.

19. M. C. Wei *et al*., *Science* **292**, 727 (2001).
20. M. E. McCurrach, T. M. Connor, C. M. Knudson, S. J. Korsmeyer, S. W. Lowe, *Proc. Natl. Acad. Sci. U.S.A.* **94**, 2345 (1997).
21. L. Zhang, J. Yu, B. H. Park, K. W. Kinzler, B. Vogelstein, *Science* **290**, 989 (2000).
22. J. E. Chipuk *et al*., unpublished data.
23. C. A. Vater, L. M. Bartle, C. A. Dionne, T. D. Littlewood, V. S. Goldmacher, *Oncogene* **13**, 739 (1996).
24. T. Kuwana *et al*., *Cell* **111**, 331 (2002).
25. A. Letai *et al*., *Cancer Cell* **2**, 183 (2002).
26. E. H. Cheng *et al*., *Mol. Cell* **8**, 705 (2001).
27. M. C. Wei *et al*., *Genes Dev.* **14**, 2060 (2000).
28. E. Yang *et al*., *Cell* **80**, 285 (1995).
29. N. N. Danial *et al*., *Nature* **424**, 952 (2003).
30. D. M. Finucane, E. Bossy-Wetzel, N. J. Waterhouse, T. G. Cotter, D. R. Green, *J. Biol. Chem.* **274**, 2225 (1999).
31. M. Suzuki, R. J. Youle, N. Tjandra, *Cell* **103**, 645 (2000).
32. Supported by NIH grants GM52735, AI47891, and AI40646 (D.R.G.). J.E.C. is supported by a Ruth L. Kirschstein National Research Service Award. We thank G. Wahl and J. Stommel for the *Trp53*^{Q5} MEF; D. Tupper and C. Giamanco for technical assistance; and all members of the Green and Newmeyer laboratories for discussions and suggestions.

Supporting Online Material
www.sciencemag.org/cgi/content/full/303/5660/1010/DC1
Materials and Methods
SOM Text
Figs. S1 to S5
References

20 October 2003; accepted 5 January 2004

Structural Basis of Transcription: Separation of RNA from DNA by RNA Polymerase II

Kenneth D. Westover, David A. Bushnell, Roger D. Kornberg*

The structure of an RNA polymerase II–transcribing complex has been determined in the posttranslocation state, with a vacancy at the growing end of the RNA-DNA hybrid helix. At the opposite end of the hybrid helix, the RNA separates from the template DNA. This separation of nucleic acid strands is brought about by interaction with a set of proteins loops in a strand/loop network. Formation of the network must occur in the transition from abortive initiation to promoter escape.

X-ray crystallography has revealed the RNA-DNA hybrid at the center of an RNA polymerase II (Pol II)–transcribing complex (*1*). Besides confirming the existence of the hybrid, previously inferred from biochemical evidence, the x-ray structure showed the orientation of the hybrid helix at an angle of almost 90° to the incoming DNA double helix, and the position of the growing end of the hybrid above an opening in the floor of the Pol II active center, through which nucleotides are thought to enter for transcription. What the x-ray structure did not reveal were the critical events at the ends of the hybrid: the selection, at the growing or downstream end, of a ribonucleotide triphosphate complementary to the coding base in the template DNA; and the separation of strands at the upstream end, whereby the product RNA is disengaged from the template DNA.

These limitations of the previous x-ray structure derived from the method of generating the transcribing complex. It involved the use of a duplex DNA with a single-stranded "tail" protruding from one 3′ end. Pol II initiates transcription on the tail, about three residues from the junction with the duplex region (*2*). The advantage of this approach is that it does not require the many general transcription factors involved in initiation at a promoter. The disadvantages are that initiation on a tailed template is imprecise, leading to heterogeneity in transcript length, and the transcript fails to separate from the template, giving rise to an extended RNA-DNA hybrid. A further limitation of the previous work was that the 3′ end of the transcript lay in the nucleotide-addition site (also known as the i+1 site). Because transcription had been paused by withholding uridine 5′-triphosphate (UTP), required for pairing with the next base in the template, the 3′ end of the transcript must have advanced by translocation to the −1 site, exposed the requirement for UTP, and then backtracked to the i+1 site. Pausing by withholding UTP was also problematic because of misincorporation, resulting in additional heterogeneity of the transcribing complex.

We have overcome these limitations by assembly of transcribing complexes from Pol II and synthetic oligonucleotides, rather than by actual transcription of DNA. Others have shown that Pol II binds a single strand of DNA and eight- or nine-residue complementary RNA to form a stable complex, capable of extending the RNA (*3*). Addition of the complementary strand of DNA results in a complete transcribing complex, capable also of separating the RNA product from the DNA.

Ten-subunit Pol II from *Saccharomyces cerevisiae* was combined with a 15-residue DNA strand and 9-residue complementary RNA. A chain-terminating residue was added to the RNA by transcription with 3′-deoxyadenosine triphosphate (Fig. 1). The resulting complex crystallized in the form of thin, fragile, radiation-sensitive plates. Data were collected to 3.6 Å resolution (Table 1), and the structure was solved by molecular replacement with the previous transcribing-complex structure and rigid body refinement (*4*). An electron density map calculated with the current x-ray intensities and phases from the previous model with the RNA and DNA removed ("omit map") showed clear density for the RNA-DNA hybrid (Fig. 1), confirming its presence in the current structure. The near identity of the current and previous structures establishes the equivalence of the complex assembled from oligonucleotides to that formed by transcription.

Where the omit map differed from the previous structure was at the upstream and downstream ends of the RNA-DNA hybrid. The omit map lacked any density at the downstream end for a nucleotide in the i+1 site [Fig. 1; compare (C) and (D)]. The complex was evidently in the "posttranslocation" state, with the nucleotide that was just added to the RNA having advanced to the −1 site, leaving the i+1 site open for addition of the next nucleotide. Elsewhere we report on the interaction of nucleotides with the i+1 site, giving insight into the nucleotide-addition mechanism (*5*).

The omit map differed from the previous transcribing-complex structure at the upstream end of the RNA-DNA hybrid by the presence of density for additional nucleic acid residues and protein loops (Fig. 2). The paths of the RNA and DNA strands clearly diverged, beginning at position −8, with residues −9 and −10 of the RNA completely separated from the complementary residues in the DNA (Fig. 2, A and B). The RNA-DNA hybrid was therefore eight base pairs in length, the same as the optimal length for stability of a complex assembled from oligonucleotides (*3*).

Three protein loops that could not be traced because of disorder in any previous polymerase structure—the "lid (Rpb1 246–264)," "rudder (Rpb1 310–324)," and "fork loop 1 (Rpb2 461–480)"—are now revealed. All three loops play key roles in RNA-DNA strand separation (Fig. 2, C and D). Ordering of these loops is evidence of their interaction with RNA, DNA, and one another in the present structure. The lid serves as a wedge to drive the RNA and DNA strands apart and interacts with residues −8, −9, and −10 of the RNA. It forms a barrier to maintain the separation of the strands and guide the RNA along an exit path. Rpb1 residue Phe^{252}, at the tip of the wedge, splits the RNA-DNA base pair at position −10, contacting the DNA base with the

Department of Structural Biology, Stanford University School of Medicine, Stanford, CA 94305–5126, USA.

*To whom correspondence should be addressed. E-mail: kornberg@stanford.edu